Superlattices and Microstructures 148 (2020) 106713

Contents lists available at ScienceDirect

Superlattices and Microstructures

journal homepage: www.elsevier.com/locate/superlattices

Importance of separating contacts from the photosensitive layer in heterojunction phototransistors

Rouzbeh Molaei Imenabadi, Ali Saadat, Trey B. Daunis, Lakshmi N.S. Murthy, Maarten L. Van de Put, Julia W.P. Hsu, William G. Vandenberghe *

Department of Materials Science and Engineering, University of Texas at Dallas, Richardson, TX, 75080, USA

A B S T R A C T —

We simulate the detection of light in solution-processed poly(3-hexylthiophene) (P3HT)-capped indium oxide (In_2O_3) phototransistors with and without direct electrical contact between the P3HT and the source and drain contacts. Under illumination, the photogenerated carriers enhance the drain current of the transistor, enabling photodetection. We demonstrate improved phototransistor performance by eliminating direct electrical contact between the P3HT and the source and drain contacts due to the inhibition of hole current flow between the contacts in the off-state. The photoresponsivity and detectivity are improved by up to 2.5 and 7 orders of magnitude, respectively, and reach a maximum of 4.4 A/W and 8.7×10^{17} Jones. Photodetection down to incident light powers as low as 5 pW/cm^2 is possible in the absence of direct contacts while detection is limited to 50 μW/cm^2 otherwise. We determine the photoresponse rise and fall time as 0.4 μs and 0.6 μs, respectively. Our study highlights the importance of using source/drain contacts that are separated from the photosensitive layer to realize optimal phototransistor performance.

1. Introduction

The ability to capture electromagnetic radiation and convert it to an electrical signal is crucial for many modern applications ranging from remote sensing to imaging, optical communications, health monitoring, night vision, object inspection, and biomedical diagnostics [1_10]. Extensive research has been performed to realize highly sensitive photodetectors with a large number of semiconductor materials, including Si, ZnO, GaN, InGaAs, conjugated polymers, nanomaterials, graphene, and other two-dimensional materials [11_21].

Amorphous indium-oxide based thin-film transistors (TFTs), including InO_x, $InZnO_x$, and $InGaZnO_x$ (IGZO) as the semiconductor, are of interest due to their compatibility with low-temperature large-area processing and their relatively high field-effect carrier mobility (more than 10 cm^2/V) [22_32]. However, because of their large optical bandgap, exceeding 3 eV, these materials only absorb high energy ultraviolet (UV) light and shorts wavelength visible-light below 420 nm [33]. At first sight, this precludes their use for photodetection applications which require the detection of visible and near IR wavelength light. Fortunately, photodetection capabilities can be expanded to visible light by fabricating heterojunction TFTs where the amorphous oxide semiconductors (α-OSs) are integrated with a visible-light absorbing capping layer [34].

Detection of visible-light with α-OSs as the active channel layer with a light-absorbing capping layer has been previously reported. For example, graphene dots, PbS quantum dots, and MoS_2 films have been demonstrated as visible-light absorbing materials. [35_37]. However, the use of dispersed nanomaterials or two-dimensional materials requires complex processing resulting in insufficient yield [35]. Semiconducting organic molecules and polymers are alternative absorbing materials which retain the low-temperature, large-area, and low-cost solution processability of α-OS TFT fabrication. As reported in Ref. [38_42], this hybrid phototransistor

* Corresponding author.
E-mail address: william.vandenberghe@utdallas.edu (W.G. Vandenberghe).

https://doi.org/10.1016/j.spmi.2020.106713
Received 7 May 2020; Received in revised form 13 September 2020; Accepted 20 September 2020
Available online 21 October 2020

structure has been used previously to improve the photosensitivity of In_2O_3 TFTs for the wavelength range of 380 nm–620 nm.

A specific heterostructure phototransistor that shows promise consists of an n-type amorphous indium gallium zinc oxide (IGZO) channel combined with a p-type organic narrow bandgap semiconductor, P3HT [39], light-absorbing material. The photodetection arises from increased channel conductivity due to photogenerated electrons injected into the high mobility IGZO channel from the P3HT following light absorption. Unfortunately, this hybrid device at present suffers from a high off-state leakage current (I_D), low photoresponsivity, and detectivity. Similar reported device structures also show detectivities and responsivities, summarized in Table S1 of the supplementary materials, that are not competitive with inorganic devices.

In this paper, we propose an underlapped source/drain (USD) TFT structure to prevent direct electrical contact between source/drain electrodes and the organic capping layer [11]. The specific TFT transfer characteristics and photodetection spectrum are determined by the α-OS and the organic capping layer materials, respectively. Here we use In_2O_3 as the semiconductor channel and P3HT as the organic capping layer as an example. We choose In_2O_3 because it is a simple binary oxide with high mobility, and P3HT because it is a common semiconducting polymer with strong absorption in the visible spectrum centered around 500 nm. However, while we use P3HT to demonstrate the device design concept; the device improvement from the new design is not specific to P3HT, but can rather apply to other absorbers. We use simulated devices to analyze the behavior of devices with and without underlap. We compute the detectivity and responsivity and find that the underlapped source/drain configuration shows a high responsivity in the visible light (500 nm) measuring around 5 A/W, with a detectivity exceeding 10^{17} Jones, and a low dark current density of 10^{-19} A/cm^2. The responsivity and detectivity values are 2.5 and 7 orders of magnitude larger, respectively, than those of the currently fabricated organic/α-OS phototransistors, highlighting the importance of using the underlapped source/drain structure.

2. Device structure and simulation parameters

The conventional organic/α-OS TFT structure, consisting of an In_2O_3 channel capped with solution-processed poly(3-hexylthiophene) (P3HT) is depicted in Fig. 1a. The modified USD TFT structure, where the source and drain contacts are not in electrical contact with the photosensitive P3HT, is shown in Fig. 1b. For our study, a 150-nm-thick silicon dioxide (SiO_2) layer acting as the gate dielectric is on top of a back-gate electrode with a work function of 4.1 eV. A 20-nm-thick high mobility (9 cm^{2}V^{-1}s^{-1}) *n*-type doped (5.0×10^{15} cm^{-3}) In_2O_3 layer on top of the SiO_2 serves as the semiconductor channel (Table S2 of supplementary material). A 50-nm-

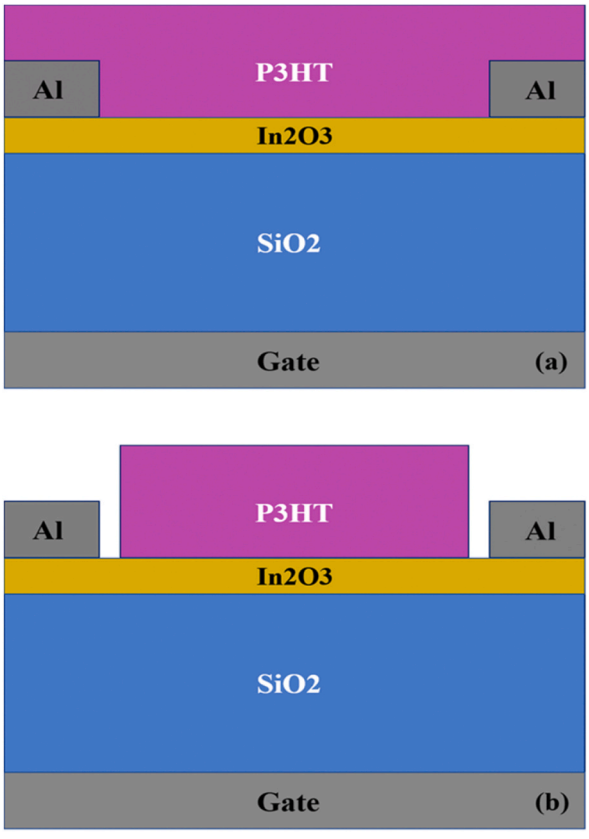

Fig. 1. Simulated device structure of the (a) conventional organic-based TFT and (b) underlapped source/drain organic-based TFT. The thickness of the photosensitive polymeric absorber layer is 100 nm. The thickness of the indium oxide channel and gate dielectric is 20 nm and 150 nm, respectively. The aluminum source and drain (labeled Al) contact lengths are 10 μm. Gate length (L_g) is 100 μm.

thick aluminum layer is used as the source and drain contacts. The device channel length and width are fixed at 100 μm and 1500 μm, respectively. Finally, a 100-nm-thick 1.0×10^{15} cm^{-3} *p*-doped P3HT layer acts as the photosensitive layer. Table S2 of supplementary material summarizes the input electrical and optical parameters for each layer.

To analyze the device characteristics, we employ numerical simulations using a commercial finite-element based two-dimensional drift-diffusion simulation package [43]. For a given device geometry, the drift-diffusion equations are solved self-consistently with the continuity equations and the Poisson equation. Since we consider an organic semiconductor, we account for the formation of excitons [44,45] and apply the singlet-exciton continuity equation to model exciton diffusion to the P3HT/In_2O_3 interface. We use a Poole-Frenkel-type field-dependent mobility model taking into account the hopping transport of the electrons and holes; $\mu = \mu_0(T)\exp(-E_0/kT)\exp(\sqrt{F}(\beta/T-\gamma))$ where $\mu_0(T)$ is the low-field mobility, and and γ are fitting parameters, E_0 is the effective activation energy, and F is the local driving force (electric field) [46,47]. A Gaussian density-of-states (DOS) is considered to approximate the effective DOS for electrons and holes in disordered organic semiconductor materials. The Langevin recombination model is used to model the recombination process of carriers and the generation process of singlet excitons in P3HT [46,47].

The spatially resolved photon absorption rates are calculated by means of an optical simulator. To obtain the light-field, optical simulations are performed using the raytracing (RT) method assuming linear polarization, as implemented in Sentaurus Device [48]. The optical generation within both the conventional and the proposed device profiles are interpolated onto the finite-element mesh adopted by the device simulator (Fig. S1 of supplementary material).

3. Results and discussion

In Fig. 2, the simulated transfer characteristics (drain current, I_D, as a function of gate voltage, V_G) are shown for both the conventional and the proposed USD P3HT/In_2O_3 phototransistors in the absence of illumination (dark) and under various illumination intensities ranging from 5 pW/cm^2 to 5 mW/cm^2. All drain currents in this study are normalized to the channel width and have units of A/mm. The observed difference between the transfer characteristics in the absence of light (dark) and under illumination shows the photodetection capabilities of these devices. In the dark, the conventional device reveals a much larger current for negative gate bias compared to the proposed device with underlapped source/drain regions.

For the conventional device, our calculations predict a subthreshold slope of 124 mV/dec, similar to what has been observed experimentally in the literature [Table S1 of supplementary material]. The proposed USD TFT, on the other hand, has a superior subthreshold slope of 68 mV/dec.

Our simulations show that the ability to detect low-intensity light in these hybrid phototransistors is determined by whether there is direct electrical contact between the polymeric photogate and the source and drain electrodes. The only desirable current path is that of electrons transported through the high mobility In_2O_3 layer. Transport through this current path is dominant for positive gate-to-source voltages where electrons dominate carrier transport. However, direct electrical contact creates an additional current path in the conventional device, which is insensitive to light illumination as evidenced by the high off-state current in the dark in Fig. 2. This second current path in conventional devices proceeds through the *p*-type P3HT channel. Holes can flow into the P3HT because of the direct electrical contact between the photosensitive gate and the electrodes. This current path is dominant for negative gate-to-source voltages where holes are the dominant carriers of current.

To better understand the difference in behavior, we show the electron concentration at positive gate bias ($V_{gs} = 5.0$ V) for both the conventional and proposed USD devices in Fig. 3. Under positive gate bias, conduction in both devices is governed by electrons and the

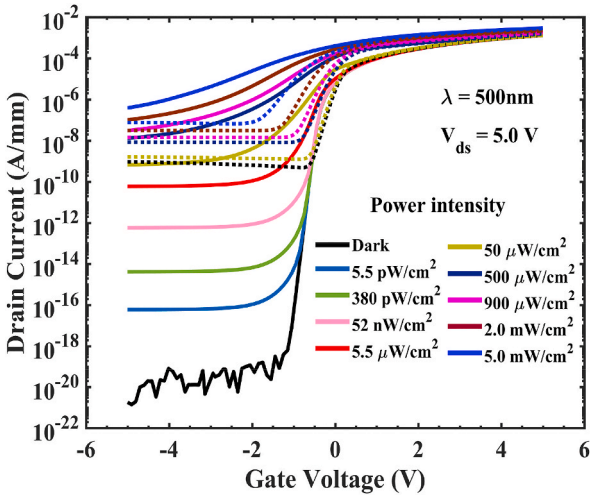

Fig. 2. Transfer characteristics of the conventional organic-based TFT (dotted lines) and underlapped source/drain organic-based TFT (solid lines) under 500 nm illumination. It can be easily seen that the conventional device just has photoresponse at light power intensities from 50 μW/cm^2 to 5.0 mW/cm^2.

current flows mostly through the *n*-type high mobility channel, which is seen from the electron density in Fig. 3. (Fig. S2 of supplementary material shows contour maps of total current density under positive gate bias). Since electron transport dominates, both devices carry very similar on-state current in the positive gate-to-source regime as is seen in Fig. 2.

To study the current flow in the negative gate-to-source regime, we show the hole concentration at negative gate bias ($V_{gs} = -5.0$ V) in Fig. 4. Both devices have similar hole concentration but in the proposed USD TFT device, the absence of a contact to the P3HT will inhibit hole current flow. In this device, the current observed in the dark is in fact still carried by electrons in the In_2O_3 (Fig. S3 of supplementary material shows the contour maps of total current density under negative gate bias).

To further clarify the picture of the two independent current paths, we simulate two separate structures, one with just the In_2O_3 and one with just the P3HT, as illustrated in the inset of Fig. 5. We add the current of the transfer characteristics of both simulations and compare the sum with the conventional device characteristics in Fig. 5. The separate devices show the same off-current and reveal that the increased off-current in the conventional device is due to a parasitic current path through the P3HT.

To quantify the promise of the USD TFT phototransistor, we determine the photoresponsivity of the organic/α-OS hybrid phototransistor by calculating the responsivity (R) and the detectivity (D*). We perform all calculations in the region $V_{gs} < 0$, where the current changes the most for both devices. More precisely we use $V_{gs} = -2$ V. The photoresponsivity (R_{ph}) is given by Refs. [39,41,49].

$$R = \frac{I_{d(illumination)} - I_{d(dark)}}{P_{in}} \tag{1}$$

where $I_{d(illumination)}$ is the drain current under illumination, $I_{d(dark)}$ is the drain current in the dark, and P_{in} is the power provided by the incident light, which is equal to the light power density times the device channel area (device channel length multiplied by channel width, 100 μm × 1500 μm in our case). Detectivity is a figure of merit characterizing the performance of photodetectors, equaling the reciprocal of the noise-equivalent-power, normalized by the square root of the sensor's area and bandwidth [49]. The detectivity is related to the responsivity by the relation [34,36,41].

$$D^* = \frac{R}{(2qI_{d(dark)}/A)^{1/2}} \tag{2}$$

where q is the elementary charge and A is the effective area of the detector.

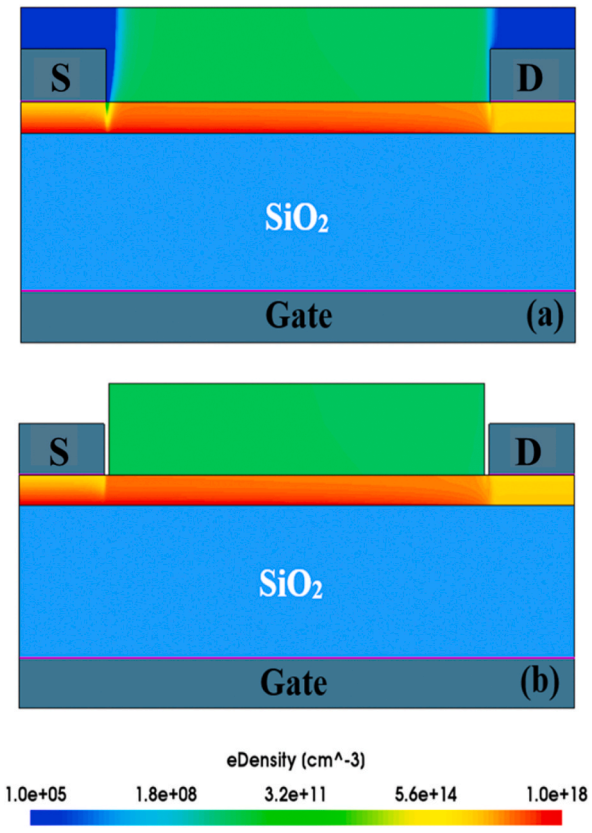

Fig. 3. Electron density of the (a) conventional organic-based TFT and (b) underlapped source/drain organic-based TFT at $V_{ds} = 5.0$ V and $V_{gs} = 5.0$ V in the dark.

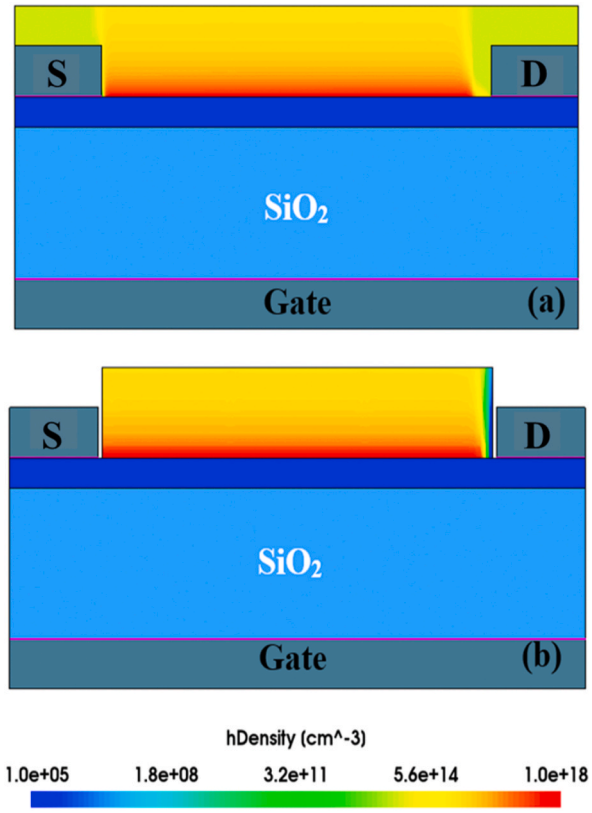

Fig. 4. Hole density of the (a) conventional organic-based TFT and (b) underlapped source/drain organic-based TFT at $V_{ds} = 5.0$ V and $V_{gs} = -5.0$ V in the dark.

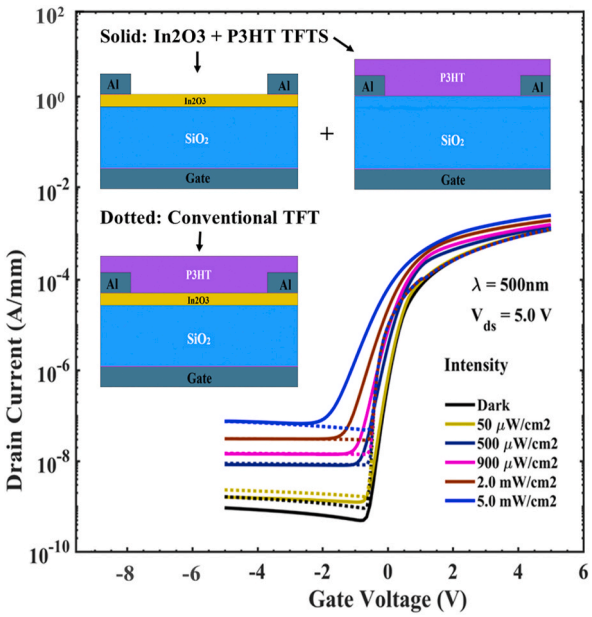

Fig. 5. Transfer performance of the conventional P3HT/In_2O_3 TFT (dotted lines) and standard In_2O_3 TFT in addition to organic-based P3HT TFT mixed together (solid lines) under 500 nm illumination.

Fig. 6 shows the photoresponsivity and detectivity at $V_{ds} = 5.0$ V and $V_{gs} = -2.0$ V as a function of illumination power density under a 500 nm light source. The performance of the proposed USD-TFT with underlapped source/drain regions is orders of magnitude better than the conventional device. Specifically, the detectivity is higher by up to 7 orders of magnitude for all ranges of the light power intensities while the responsivity is higher by roughly 2.5 orders of magnitude at high power densities (0.5 mW/cm^2 to 5.0 mW/cm^2). The proposed device realizes a maximum responsivity of 4.4 A/W at a light power density of 5 mW/cm^2, approximately 367 times higher than the conventional one (1.17×10^{-2} A/W). The detectivity at this power measures 8.7×10^{17} Jones for the proposed device compared to 1.16×10^{10} Jones for the conventional device. The sudden increase in responsivity and detectivity for the proposed device above 10^{-5} W/cm^2 light power intensity is due to the negative shift in the transistor on voltage (V_{ON}) with increasing illumination power. For illumination greater than 10^{-5} W/cm^2 V_{ON} becomes less than −2 V so the illumination I_D is greater than the off-current. This effect becomes more pronounced with V_{ON} decreasing further with higher illumination intensities, so responsivity and detectivity continue to increase. For the conventional device, V_{ON} never decreases below −2 V even for the highest illumination intensity (5 mW/cm^2), so responsivity and detectivity remain relatively flat versus power intensity.

Both the conventional device and the USD device exhibit maximal responsivity at the highest power intensity simulated (5.0 mW/cm^2), and both devices maintain good responsivity down to very low power intensity (5.5 pW/cm^2). However, it is important to note that current is not visibly different for power intensities below 50 μW/cm^2 in the conventional device. The non-vanishing responsivities and detectivities that we compute in the conventional device are the result of differences in current that are very small and not visible in Fig. 2.

The results shown in Fig. 6 assume a 500 nm light source; we repeat our responsivity calculations for the proposed USD device for a 5 mW/cm^2 light source with a wavelength ranging from 250 nm to 700 nm. (Fig. S4 of the supplementary material). Responsivity increases with increasing wavelength up until 500 nm after which responsivity declines. In other words, responsivity reaches its peak value at a wavelength of 500 nm due to the light absorbance spectrum of the P3HT capping layer [50]. Moreover, the In_2O_3 channel and the P3HT capping layer are almost transparent to light with a wavelength longer than 650 nm. Comparing these simulations with recently reported α-OS based phototransistors with nano, perovskite, or organic materials [Table S1 of supplementary material], we see significantly improved performance in the detectivity and transient response.

To study the transient response of the phototransistor with underlapped source/drain regions, we simulate a periodic illumination with a 30 μs period and 5 μs light-on time with light power intensities of 95, 320, 675 nW/cm^2, as shown in Fig. 7. The drain current was extracted at $V_{ds} = 5.0$ V and $V_{gs} = -2.0$ V. A fast transient response is observed with an abrupt rise and fall in I_D and a high $I_{light\text{-}on}/I_{light\text{-}off}$ ratio (10^7). This fast transient response shows that our devices as simulated are not plagued with any considerable amount of persistent photoconductivity, compared to, for example the continuous increase under pulse illumination observed in Ref. [34].

To quantify the response time, a magnified figure of the rise and fall of the response periods are plotted in Fig. 7b and (c). From these figures, we extract the rise and fall times, defined as the time interval between 10% and 90% of the peak value of the photocurrent when light is on and off [34,36]. A 0.4 μs rise time and a 0.6 μs fall time under 675 nW/cm^2 is extracted. These rise and fall times meet the specifications needed for sensing and imaging applications [34,36]. The simulated response time is several orders of magnitude faster than several recently reported hybrid phototransistors with nano and organic materials, such as graphene nanosheets/IGZO, MoS_2/IGZO, and P3HT/IGZO [35–42] (Table S1 of supplementary material).

We have studied an idealized version of the proposed device with underlapped source/drain regions, where the contacts are completely insulated from the photosensitive layer through the removal of a small section of the photosensitive material next to the contact. In a physical implementation, such complete electrical insulation is difficult to realize. A more practical implementation may proceed by covering the source and drain electrodes with a thin layer of insulating material [11], e.g. silicon nitride, before deposition

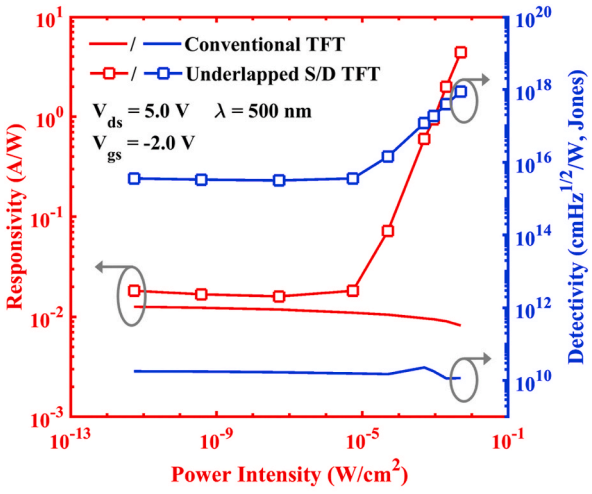

Fig. 6. Optical power dependencies of the photoresponsivity (red, left axis), detectivity (blue, right axis) of the conventional TFT (line only) and USD TFT (squares + line) at $V_{ds} = 5.0$ V and $V_{gs} = -2.0$ V.

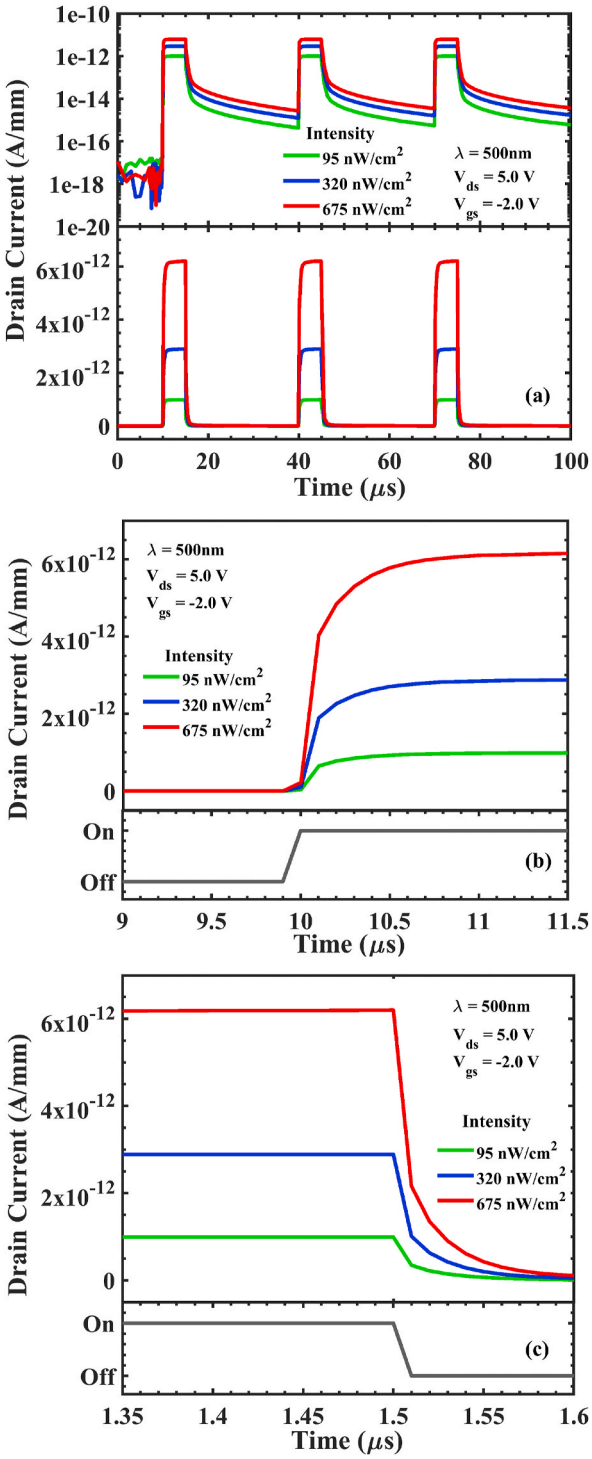

Fig. 7. (a) Logarithmic plot (top panel) and linear plot (bottom panel) of the time-dependent photo-response characteristics of the proposed USD TFT under a 500 nm incident pulse light at $V_{ds} = 5.0$ V and $V_{gs} = -2.0$ V, respectively. (b–c) The enlarged figures of one cycle of Fig. 7(a) bottom panel (which is the linear plot of the time-dependent photo-response characteristics of the proposed USD TFT), showing the (b) rise time and (c) fall time of the proposed underlapped In_2O_3/P3HT TFT under 500 nm incident light.

of the P3HT. The ideal device with fully insulated source/drain regions electrical behavior including total current density is studied in Fig. S5 of the supplementary material. Interestingly, the electrical behavior of these insulated source/drain device and ideally insulated USD device discussed above is almost the same.

4. Conclusion

In conclusion, we have simulated a solution-processed phototransistor where an In_2O_3 channel is capped with a P3HT polymeric photoabsorbing layer. We have proposed a device structure with underlapped source/drain regions. We found that P3HT capped In_2O_3 TFTs with underlapped source/drain regions maintain a low off-current below 10^{-18} A/mm, an on/off-current ratio of over 10^{13}. Responsivities and detectivities exceeding 4 A/W and 10^{17} Jones were found respectively, well in excess of previously reported papers for hybrid phototransistors. Our research shows that hybrid phototransistor performance can be drastically improved by preventing direct electrical contact between source/drain electrodes and the photosensitive layer, hence reducing off-current in the dark.

Author statement

Rouzbeh Molaei Imenabadi: Methodology, Investigation, Writing - original draft. Ali Saadat: Validation, Writing - review & editing. Trey B. Daunis: Validation, Writing - review & editing. Lakshmi N. S. Murthy: Writing - review & editing. Maarten L. Van de Put: Supervision, Writing - review & editing. Julia. W. P. Hsu: Conceptualization, Funding acquisition, Supervision, Writing - review & editing. William G. Vandenberghe: Methodology, Conceptualization, Funding acquisition, Supervision, Writing - review & editing.

Declaration of competing interest

The authors declare that they have no known competing financial interests or personal relationships that could have appeared to influence the work reported in this paper.

Acknowledgment

This work is supported at the University of Texas at Dallas Texas Photonic Center and partially supported by National Science Foundation (CBET-1916612). JWPH acknowledges the Texas Instruments Distinguished Chair in Nanoelectronics.

Appendix A. Supplementary data

Supplementary data to this article can be found online at https://doi.org/10.1016/j.spmi.2020.106713.

References

[1] R. Soref, The impact of silicon photonics, IEICE Trans. Electron. E91.C (2008) 129–130.
[2] J.H. Lee, D.H. Kim, D.J. Yang, S.Y. Hong, K.S. Yoon, P.S. Hong, C.O. Jeong, H.S. Park, S.Y. Kim, S.K. Lim, S.S. Kim, K.S. Son, T.S. Kim, J.Y. Kwon, S.Y. Lee, World's largest (15- in.) XGA AMLCD panel using IGZO oxide TFT, Dig. Tech. Pap. Soc. Inf. Disp. Int. Symp. 39 (2008) 625–628.
[3] R.A. Lujan, R.A. Street, Flexible X-ray detector array fabricated with oxide thin-film transistors, IEEE Electron. Device Lett. 33 (2012) 688–690.
[4] G. Konstantatos, E.H. Sargent, Nanostructured materials for photon detection, Nat. Nanotechnol. 5 (2010) 391–400.
[5] A. Rogalski, J. Antoszewski, L. Faraone, Third-generation infrared photodetector arrays, J. Appl. Phys. 105 (2009), 091101.
[6] F.P.G. Arquer, A. Armin, P. Meredith, E.H. Sargent, Solution-processed semiconductors for next-generation photodetectors, Nat. Rev. Mater. 2 (2017) 16100.
[7] C. Zhao, J. Kanicki, Amorphous In-Ga-Zn-O thin-film transistor active pixel sensor x-ray imager for digital breast tomosynthesis, Med. Phys. 41 (2014), 091902.
[8] A.R. Hawkins, W. Wu, P. Abraham, K. Streubel, J.E. Bowers, High gain-bandwidth-product silicon heterointerface photodetector, Appl. Phys. Lett. 70 (1997) 303.
[9] Y. Kang, H.D. Liu, M. Morse, M.J. Paniccia, M. Zadka, S. Litski, G. Sarid, A. Pauchard, Y.H. Kuo, H.W. Chen, W.S. Zaoui, J.E. Bowers, A. Beling, D.C. McIntosh, X. Zheng, J.C. Campbell, Monolithic germanium silicon avalanche photodiodes with 340GHz gain-bandwidth product, Nat. Photon. 3 (2008) 59–63.
[10] Y. Gao, H. Cansizoglu, K.G. Polat, S. Ghandiparsi, A. Kaya, H.H. Mamtaz, A.S. Mayet, Y.A. Wang, X.Z. Zhang, T. Yamada, E.P. Devine, A.F. Elrefaie, S.Y. Wang, M.S. Islam, photon-trapping microstructures enable high-speed high-efficiency silicon photodiodes, Nat. Photon. 11 (2017) 301–308.
[11] V. Adinolfi, E.H. Sargent, Photovoltage field-effect transistors, Nat 542 (2017) 324–327.
[12] E. Muñoz, E. Monroy, J.a. Garrido, I. Izpura, F.J. Sanchez, M.A. Sanchez-Garcia, E. Calleja, B. Beaumont, P. Gibart, Photoconductor gain mechanisms in GaN ultraviolet detectors, Appl. Phys. Lett. 71 (1997) 870–872.
[13] B. Nie, J.-G. Hu, L.-B. Luo, C. Xie, L.-H. Zeng, P. Lv, F.-Z. Li, J.-S. Jie, M. Feng, C.-Y. Wu, Y.-Q. Yu, S.-H. Yu, Monolayer graphene film on ZnO nanorod array for high-performance Schottky junction ultraviolet photodetectors, Small 9 (2013) 2872–2879.
[14] S.J. Xu, S.J. Chua, T. Mei, X.C. Wang, X.H. Zhang, G. Karunasiri, W.J. Fan, C.H. Wang, J. Jiang, S. Wang, X.G. Xie, Characteristics of InGaAs quantum dot infrared photodetectors, Appl. Phys. Lett. 73 (1998) 3153–3155.
[15] X. Gong, M. Tong, Y. Xia, W. Cai, J.S. Moon, Y. Cao, G. Yu, C.-L. Shieh, B. Nilsson, A.J. Heeger, High-detectivity polymer photodetectors with spectral response from 300 to 1450 nm, Science 325 (2009) 1665–1667.
[16] X. Huang, C. Wu, H. Lu, F. Ren, Q. Xu, H. Ou, R. Zhang, Y. Zheng, Monochromatic light-assisted erasing effects of In-Ga-Zn-O thin film transistor memory with Al2O3/Zn-doped Al2O3/Al2O3 stacks, Appl. Phys. Lett. 100 (2012) 243505.
[17] F. Xia, T. Mueller, Y. Lin, A. Valdes-Garcia, P. Avouris, Ultrafast graphene photodetector, Nat. Nanotechnol. 4 (2009) 839–843.
[18] O. Lopez-Sanchez, D. Lembke, M. Kayci, A. Radenovic, A. Kis, Ultrasensitive photodetectors based on monolayer MoS2, Nat. Nanotechnol. 8 (2013) 497–501.
[19] L. Xu, R.M. Imenabadi, W. Vandenberghe, J.W.P. Hsu, Minimizing performance degradation induced by interfacial recombination in perovskite solar cells through tailoring of the transport layer electronic properties, Appl. Phys. Lett. 122 (2018) 15140–15148.

[20] J. Wang, L. Xu, B. Zhang, Y.J. Lee, J.W.P. Hsu, N-type doping induced by electron transport layer in organic photovoltaic devices, Adv. Electron. Mater. 3 (2017) 1600485.
[21] R.M. Imenabadi, M.L. Van de Put, T.B. Daunis, L. Xu, N.S. Murthy, J.W.P. Hsu, W. Vandenberghe, Indium oxide-based photo field-effect transistor with polymeric photosensitive gate, IEEE. SISC. 5 (2017) 435–437.
[22] M.C. Chen, T.C. Chang, C.T. Tsai, S.Y. Huang, S.C. Chen, C.W. Hu, S.M. Sze, M.J. Tsai, Influence of electrode material on the resistive memory switching property of indium gallium zinc oxide thin films, Appl. Phys. Lett. 96 (2010) 262110.
[23] E. Fortunato, P. Barquinha, R. Martins, Oxide semiconductor thin-film transistors. A review of recent advances, Adv. Mater. 24 (2012) 2945–2986.
[24] S. Jeong, J. Moon, J. Mater, Low-temperature, solution-processed metal oxide thin film transistors, Inside Chem. 22 (2012) 1243–1250.
[25] C.H. Kim, Y.H. Jang, H.J. Hwang, C.H. Song, Y.S. Yang, H. Cho, Bistable resistance memory switching effect in amorphous InGaZnO thin films, Appl. Phys. Lett. 97 (2010), 062109.
[26] S.J. Kim, S. Yoon, H.J. Kim, Review of solution-processed oxide thin-film transistors, Jpn. J. Appl. Phys. 53 (2014), 02BA02.
[27] J.S. Park, T.W. Kim, D. Stryakhilev, J.S. Lee, S.G. An, Y.S. Pyo, D.B. Lee, Y.G. Mo, D.U. Jin, H.K. Chung, Flexible full color organic light-emitting diode display on polyimide plastic substrate driven by amorphous indium gallium zinc oxide thin-film transistors, Appl. Phys. Lett. 95 (2009), 013503.
[28] Z. Wang, H. Xu, Z. Li, X. Zhang, Y. Liu, Y. Liu, Flexible resistive switching memory device based on amorphous InGaZnO film with excellent mechanical endurance, IEEE Electron. Device Lett. 32 (2011) 1442–1444.
[29] X. Yan, H. Hao, Y. Chen, Y. Li, W. Banerjee, Highly transparent bipolar resistive switching memory with In-Ga-Zn-O semiconducting electrode in In-Ga-Zn-O/Ga2O3/In-Ga-Zn-O structure, Appl. Phys. Lett. 105 (2014), 093502.
[30] W. Xu, D. Liu, H. Wang, L. Ye, Q. Miao, J.B. Xu, Facile passivation of solution-processed InZnO thin-film transistors by octadecylphosphonic acid self-assembled monolayers at room temperature, Appl. Phys. Lett. 104 (2014) 173504.
[31] W. Xu, H. Wang, L. Ye, J. Xu, The role of solution-processed high-κ gate dielectrics in electrical performance of oxide thin-film transistors, J. Mater. Chem. C 2 (2014) 5389.
[32] H. Wang, W. Xu, S. Zhou, F. Xie, Y. Xiao, L. Ye, J. Chen, J. Xu, Oxygen plasma assisted high performance solution-processed Al2Ox gate insulator for combustion-processed InGaZnOx thin film transistors, J. Appl. Phys. 117 (2015), 035703.
[33] C.S. Chuang, T.C. Fung, B.G. Mullins, K. Nomura, T. Kamiya, H.P.D. Shieh, H. Hosono, J. Kanicki, Photosensitivity of amorphous IGZO TFTs for active-matrix flat-panel displays, Dig. Tech. Pap. - Soc. Inf. Disp. Int. Symp. 39 (2008) 1215–1218.
[34] S. Du, G. Li, X. Cao, Y. Wang, H. Lu, S. Zhang, C. Liu, H. Zhou, Oxide semiconductor phototransistor with organolead trihalide perovskite light absorber, Adv. Electron. Mater. 3 (2017) 1600325.
[35] Z. Pei, H.-C. Lai, J.-Y. Wang, W.-H. Chiang, C.-H. Chen, High responsivity and high-sensitivity graphene dots/a-IGZO thin-film phototransistor, IEEE Electron. Device Lett. 36 (2015) 44–46.
[36] J. Yang, H. Kwak, Y. Lee, Y.S. Kang, M.H. Cho, J.H. Cho, Y.H. Kim, S.J. Jeong, S. Park, H.J. Lee, H. Kim, MoS2–InGaZnO heterojunction phototransistors with broad spectral responsivity, ACS Appl. Mater. Interfaces 8 (2016) 8576–8582.
[37] D.K. Hwang, Y.T. Lee, H.S. Lee, Y.J. Lee, S.H. Shokouh, J. Kyhm, J. Lee, H.H. Kim, T.H. Yoo, S.H. Nam, D.I. Son, B.K. Ju, M.C. Park, J.D. Song, W.K. Choi, S. Im, Ultrasensitive PbS quantum-dot-sensitized InGaZnO hybrid photoinverter for near-infrared detection and imaging with high photogain, NPG Asia Mater. 8 (2016) e233.
[38] J.M. Shaw, P.F. Seidler, Organic electronics: introduction, IBM J. Res. Dev. 45 (2001) 1.
[39] H.W. Zan, W.T. Chen, H.W. Hsueh, S.C. Kao, M.C. Ku, C.C. Tsai, H.F. Meng, Amorphous indium-gallium-zinc-oxide visible-light phototransistor with a polymeric light absorption layer, Appl. Phys. Lett. 97 (2010) 203506.
[40] J. Li, F. Zhou, H.-P. Lin, W.-Q. Zhu, J.-H. Zhang, X.-Y. Jiang, Z.-L. Zhang, Enhanced photosensitivity of InGaZnO-TFT with a CuPc light absorption layer, Superlattice. Microst. 51 (2012) 538–543.
[41] H. Wang, Y. Xiao, Z. Chen, W. Xu, M. Long, J.B. Xu, Solution-processed PCDTBT capped low-voltage $InGaZnO_x$ thin film phototransistors for visible-light detection, Appl. Phys. Lett. 106 (2015) 242102.
[42] H.W. Zan, H.W. Hsueh, S.C. Kao, W.T. Chen, M.C. Ku, W.W. Tsai, C.C. Tsai, H.F. Meng, New polymer-capped a-IGZO TFT with high sensitivity to visible light for the development of integrated touch sensor array, Dig. Tech. Pap. - Soc. Inf. Disp. Int. Symp. 41 (2010) 1316.
[43] Synopsys Inc., Sentaurus Device User Guide, F-2011.09, Mountain View, CA, USA, September 2011.
[44] A. Bolognesi, A. Di Carlo, P. Lugli, Influence of carrier mobility and contact barrier height on the electrical characteristics of organic transistors, Appl. Phys. Lett. 81 (2002) 4646.
[45] A. Bolognesi, M. Berliocchi, M. Manenti, A. Di Carlo, P. Lugli, K. Lmimouni, C. Dufour, Effects of grain boundaries, field-dependent mobility, and interface trap States on the electrical Characteristics of pentacene TFT, IEEE Trans. Electron. Dev. 51 (2004) 1997–2003.
[46] K. Melzer, M. Brandlein, D. Popescu, P. Lugli, G. Scarpa, Characterization and simulation of electrolyte-gated organic field-effect transistors, Faraday Discuss 174 (2014) 399–411.
[47] S. Toffanin, R. Capelli, W. Koopman, G. Generali, S. Cavallini, A. Stefani, D. Saguatti, G. Ruani, M. Muccini, Organic light-emitting transistors with voltage-tunable lit area and full channel illumination, Laser Photon. Rev. 7 (2013) 1011–1019.
[48] M. Peters, M. Rüdiger, B. Bläsi, W. Platzer, Electro – optical simulation of diffraction in solar cells, Optic Express 18 (2010) A584–A593.
[49] A. Adinolfi, Solution Processed Hybrid Materials for Light Detection, Ph.D. thesis, University of Toronto, Canada, 2016.
[50] Z. Liang, M.O. Reese, B.A. Gregg, Chemically treating poly(3-hexylthiophene) defects to improve bulk heterojunction photovoltaics, ACS Appl. Mater. Interfaces 3 (2011) 2042–2050.